Korean J. Chem. Eng., **17**(6), 643-648 (2000)

Crystallization of High Purity Ammonium Meta-Tungstate for Production of Ultrapure Tungsten Metal

Cheong-Song Choi†, Jun-Hyung Kim* and Choul-Ho Lee**

Dept. of Chemical Engineering, Sogang University, C.P.O Box 1142, Seoul, Korea
*Agency for Defense Development, Taejon 305-600, Korea
**Dept. of Chemical Engineering, Kongju National University, Kongju 314-701, Korea
(*Received 18 May 2000 • accepted 10 June 2000*)

Abstract–The growth mechanism of Ammonium Meta-Tungstate (AMT) crystal was interpreted as two-step model. Growth rates of AMT crystals were measured in a fluidized bed crystallizer. The effects of temperature, supersaturation and crystal size on the crystal growth were investigated. The contribution of the diffusion step increased with the increase of temperature, crystal size and supersaturation. The nucleation kinetics from measurements on the width of the metastable region of Ammonium Meta-Tungstate (AMT) was also evaluated. The crystal size distribution from a programmed cooling crystallization system was predicted by the numerical simulation of a mathematical model using the kinetics of nucleation and crystal growth. It was also observed that the shape of AMT crystals was changed during the growth period.

Key words: Ammonium Meta-Tungstate, Crystallization, Process Control, Crystal Growth, Crystal Size Distribution

INTRODUCTION

Ammonium Meta-Tungstate (AMT) is commercially significant because of its high solubility in water, a property which makes it a very desirable starting material for catalysts. High purity WO_3 can also be obtained by the thermal decomposition of AMT [French and Sale, 1981]. Other uses include nuclear shielding, corrosion inhibitors, and the preparation of other tungsten chemicals. However, despite the extensive usage of AMT, there is virtually no data concerning the kinetics of the crystallization of AMT from an aqueous solution. This investigation is concerned with finding an optimal operating condition and its implementation in a batch cooling crystallizer for producing highly pure AMT crystals, which will be utilized as tungsten raw material in order to produce ultrapure tungsten metal powder.

EXPERIMENTAL

1. Crystal Shape Factors

The surface and volume shape factors for the AMT crystals were determined with a microscope fitted with a calibrated eyepiece. The length, breadth and thickness of the crystal were sized.

2. Nucleation Measurements

The experimental method used for the nucleation measurements was similar to that used earlier by Mullin and Ang [1976]. The solution was prepared from recrystallized crystals of LR grade AMT in distilled water. A solution of known saturation temperature was agitated for 1 hour at 10 °C above the saturation temperature and cooled in a 100 cm^3 crystallizer, and the temperature at which nuclei first appear was measured. The supersaturation was determined by subtracting the solubility from the actual concentration. This procedure was repeated for different cooling rates and saturation temperatures with both unseeded and seeded solutions. The equilibrium data of AMT in the binary system AMT-Water over the experimental temperature range, 10-30 °C, were determined by the polythermal method [Nyvlt, 1977; Choi and Kim, 1990]. The solubility was expressed as the relation

$$C_s = -0.000433899\,\theta^2 + 0.197532\,\theta - 0.490991 \quad (1)$$

where C_s is the solubility (in kg AMT/kg H_2O) at temperature θ (in °C).

3. Growth Experiments

The schematic diagram of the crystallizer used is shown in Fig.

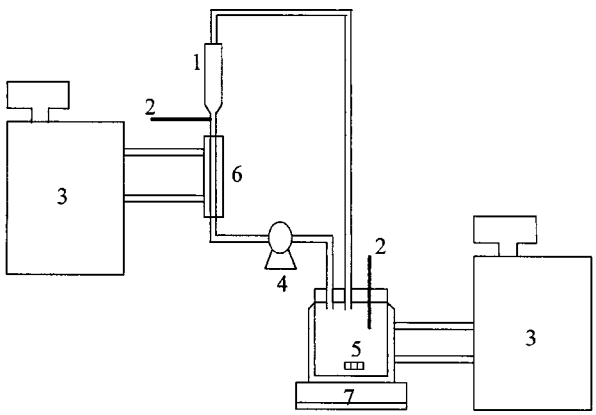

Fig. 1. Experimental apparatus.
1. Fluidized-bed crystallizer
2. Thermometer
3. Water bath
4. Pump
5. Dissolver
6. Heat exchanger
7. Magnetic stirrer

†To whom correspondence should be addressed.
E-mail: cschoi@sogang.ac.kr
This paper was presented at The 5th International Symposium on Separation Technology-Korea and Japan held at Seoul between August 19 and 21, 1999.

Table 1. Range of variables studied in growth experiments

Variables	Range	Units
Relative supersaturation, $\Delta C/C_s$	0.015 to 0.150	
Temperature	16.5 to 25.5	°C
Seed size	500 to 1700	μm

1. It was constructed mainly of glass of a diameter of 0.8 cm and a working volume of 20 cm^3. A solution of known concentration was prepared in the dissolver (5) and was circulated by a variable speed gear pump (4) controlled so that the seed crystals were uniformly fluidized. The volume of the dissolver was 2,000 cm^3 and the temperature of the solution in the dissolver was maintained 10 °C higher than that in the crystallizer in order to dissolve the nuclei which could be created in the crystallizer. The temperature of the solution entering the crystallizer was controlled by means of a heat exchanger (6) within 0.05 °C precision during the run. Seed crystals were obtained by recrystallization in a stirred tank cooling crystallizer and the crystal size was measured under an optical microscope. After the seed crystals were grown for a definite time, the product crystals were removed from the crystallizer, dried, and carefully sized. The ranges of variables studied are given in Table 1.

4. Controlled Cooling Crystallization

Batch crystallizers generally yield a poor quality product, which is mainly due to the use of a high cooling rate in the initial stages of the process, resulting in the formation of large numbers of crystal nuclei that cannot grow to the desired size. This can be overcome by an appropriate temperature control. That is, to maintain the supersaturation level within the maximum allowable supersaturation, the working supersaturation level must be low in the initial stages of the operation and can be increased as time passes--the reverse of "natural cooling". This mode of operation is termed "controlled cooling".

Batch crystallization experiments were performed in a draft-tube baffled cooling crystallizer as shown in Fig. 2. It was equipped with a hollow draft-tube and jacket through both of which the cooling water can be circulated. The agitation was provided by a propeller stirrer located on the center line of the draft-tube. The temperature was controlled by using a Lauda RUL-40D and a PMP 351-1 temperature programmer with a remote sensor. During each run the crystals were maintained essentially within the annular growth zone (between the draft-tube and the crystallizer wall) by controlling the agitation rate in order to achieve similar conditions in the liquid fluidized bed crystallizer [Choi and Kim, 1991]. At the end of each run a crystal size analysis was performed.

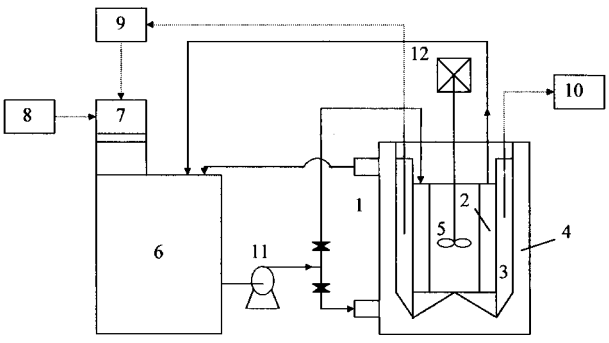

Fig. 2. Programmed cooling crystallizer.

1. Draft-tube baffled crystallizer
2. Hollow draft tube
3. Vertical wall baffles
4. Cooling water jacket
5. Three-blade screw
6. Bath reservoir
7. Temperature controller
8. Temperature programmer
9. Remote sensor
10. Recorder
11. Pump
12. Agitation speed controller

RESULTS AND DISCUSSION

1. Crystal Shape Factors

It was observed that the prepared AMT crystals in a mixed crystallizer formed truncated octahedron crystals and shape factors of crystals grown were size-dependent. Shape-size correlations are given in Fig. 3 for crystals smaller than 2.0 mm. AMT first forms small octahedron crystals, but at larger sizes the crystals tend to be-

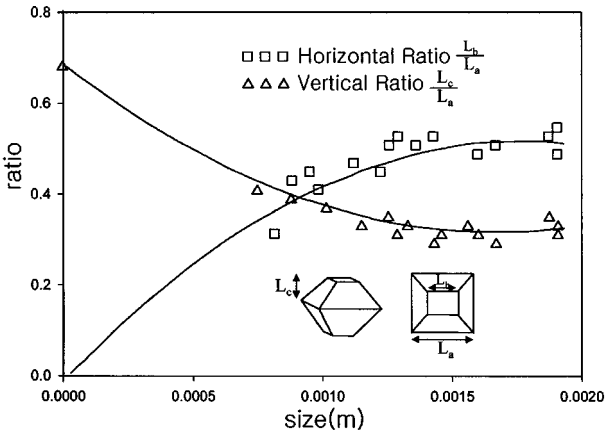

Fig. 3. Horizontal ratio and vertical ratio vs. crystal size.

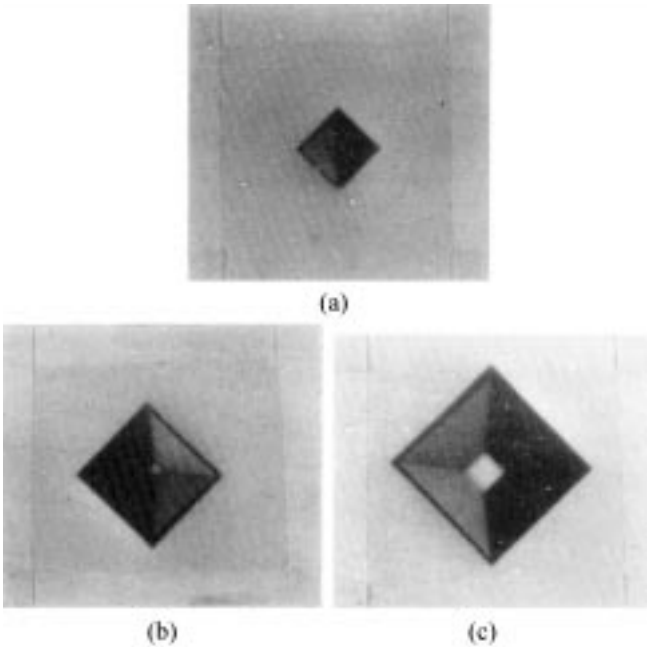

Fig. 4. Steps of shape modification of AMT crystal.
(a) Time a (b) Time b (c) Time c (Time a<Time b<Time c).

come more truncated. Fig. 4 shows the transformations into the truncated crystal through habit modification during the growth. The volume and surface shape factors of a crystal, characterized by its characteristic size, L (=L_a in Fig. 3), are given by

$$f_v = -1.08\,L^5 + 5.14\,L^4 - 5.19\,L^3 - 4382.5\,L^2 - 15.4\,L + 0.34 \quad (2)$$

and

$$f_s = -4.94\,L^4 + 3.33\,L^3 - 511341\,L^2 - 90.4\,L + 3.37 \quad (3)$$

respectively. Values of shape factors are used when the linear growth rate, G, of crystals is calculated. This is related to the mass growth rate, M_g, by

$$G = \frac{f_s}{3 f_v \rho_c} M_g = k_G (\Delta C / C_s)^g \quad (4)$$

2. Nucleation Kinetics

The semiempirical relationship, Eq. (5), has frequently been used to relate the mass nucleation rate, J_m, to the metastable zone width [Mullin and Ang, 1976; Nyvlt, 1972; Nyvlt and Söhnel, 1975]

$$J_m = k_n \left(\frac{\Delta C_{max}}{C_s} \right)^n \quad (5)$$

The mass nucleation rate coefficient, k_n, usually depends on temperature, hydrodynamic conditions and presence of impurities. The temperature dependence of k_n could be estimated by using an Arrhenius-type equation of the following form

$$k_n = k_n^o \exp(-E_n / R_g T) \quad (6)$$

At the "metastable limit" the mass nucleation rate is equal to the rate of creation of saturation due to cooling, that is,

$$J_m = k_n \left(\frac{\Delta C_{max}}{C_s} \right)^n = \frac{dC_s}{d\theta} \frac{d\theta}{dt} = \frac{dC_s}{d\theta} b \quad (7)$$

where $dC_s/d\theta$ is the temperature dependence of solubility and b is cooling rate [Jones and Mullin, 1973]. Converting to natural logarithms in Eq. (7) gives the following equation:

$$\ln(b) = -\ln(dC_s/d\theta) + \ln(k_n) + n \ln(\Delta C_{max}/C_s) \quad (8)$$

This linear expression indicates the dependence of ln(b) on ln ($\Delta C_{max}/C_s$). The slope is the "order" of the process, n, and the mass nucleation rate coefficient, k_n, can be obtained from the intercept.

1. Primary Nucleation

The data of cooling rate, b, vs. maximum allowable relative supersaturation, $\Delta C_{max}/C_s$, are plotted as shown in Fig. 5 for the four saturation temperatures studied (16.8, 19.1, 25.4 and 28.0 °C). The $\Delta C_{max}/C_s$ increases as the cooling rate increases from 6 to 20 °C/h. By substituting these values into Eq. (8), the nucleation parameters (n and k_n) can be calculated. The primary nucleation rate may be described by the expression

$$J_m = 1.6 \times 10^{39} \exp(-2.81 \times 10^5 / R_g T)(\Delta C / C_s)^{3.15} \quad (9)$$

The surface energy could be calculated from the nucleation data by means of the theory of nucleation. From the classical nucleation theory the induction period, τ, may be expressed by

$$\tau = K \exp\left(\frac{\beta \gamma^3 M_w^2 N}{(\rho_c \upsilon)^2 (R_g T)^3 (\ln S)^2} \right) = \Delta T_{max} / b \quad (10)$$

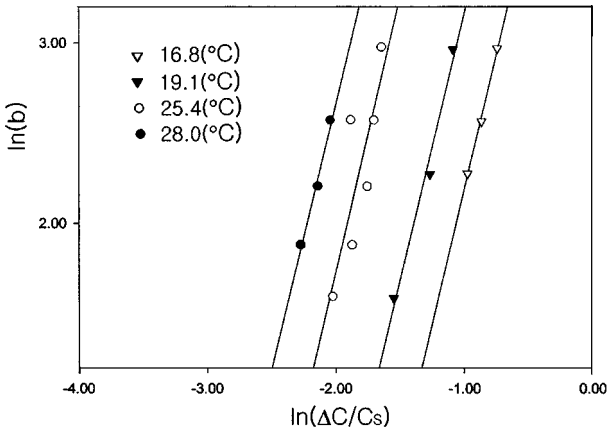

Fig. 5. Cooling rate b vs. maximum relative supersaturation for primary nucleation.

where the induction period was assumed to be inversely proportional to the nucleation rate and ΔT_{max} is the maximum allowable temperature [Nielsen, 1964]. From Eq. (7), the following relation is obtained.

$$b = k_n (\Delta C_{max}/C_s)^n / (dC_s/d\theta) \quad (11)$$

The surface energy, γ, calculated from nucleation rate measurements is 4.16 erg/cm^2.

2. Secondary Nucleation

The data of cooling rate, b, vs. maximum allowable relative supersaturation, $\Delta C_{max}/C_s$, are arranged as shown in Fig. 6 for the secondary nucleation. As shown in Fig. 6, the maximum allowable supersaturation is reduced for secondary nucleation. Like the primary nucleation, the secondary nucleation rate can be written by the expression

$$J_m = 1.7 \times 10^{41} \exp(-2.079 \times 10^5 / R_g T)(\Delta C / C_s)^{3.57} \quad (12)$$

3. Crystal Growth Kinetics

Crystal growth from solution is often considered to be a two-step growth process, that is, the crystal growth process consists of two consecutive stages [Krpata and Söhnel, 1974; Mullin and Gaska, 1969]:

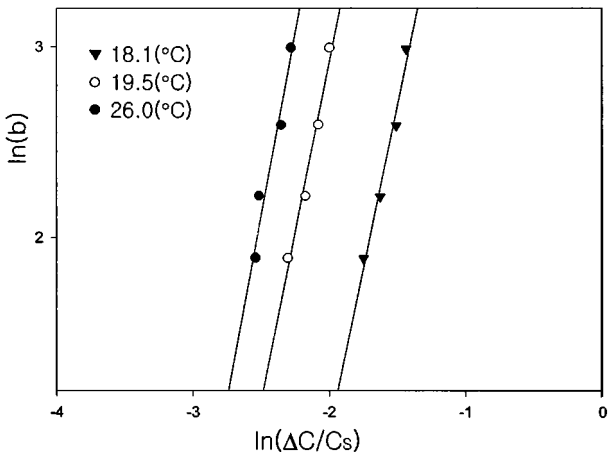

Fig. 6. Cooling rate b vs. maximum relative supersaturation for secondary nucleation.

(i) Bulk diffusion:

$$M_g = k_d\left(\frac{C - C_i}{C_s}\right) \tag{13}$$

(ii) Surface reaction:

$$M_g = k_r\left(\frac{C_i - C_s}{C_s}\right)^r \tag{14}$$

An elimination of the interfacial concentration, C_I, from the above equations gives

$$\left(\frac{M_g}{k_r}\right)^{1/r} + \left(\frac{M_g}{k_d}\right) = \frac{\Delta C}{C_s} \tag{15}$$

where r can have values between 0.83 and about 5 for a "nuclei above nuclei" (NAN) model and between 1 and 2 for the BCF model [Garside et al., 1975]. The effects of the crystal size and temperature can be incorporated in a surface reaction rate constant, k_r, and in a diffusion rate constant, k_d. The size dependence of the rate constants may be expressed by a power law term as in the Bransom growth rate model. The effect of temperature may be expressed by an Arrhenius type relation. Therefore, k_d and k_r may be expressed in the form

$$k_d = k_d^o L^{b1} \exp(-E_{gd}/R_g T) \tag{16}$$

and

$$k_r = k_r^o L^{b2} \exp(-E_{gr}/R_g T) \tag{17}$$

respectively.

Fig. 7 shows the variation of linear growth rate with concentration driving force, $\Delta C/C_s$, with 1.21 mm crystal size. The effect of temperature is shown. Growth rate increases with both supersaturation and temperature. The relation represented by Eq. (4) was used to evaluate g and k_G. The exponent g of $\Delta C/C_s$ decreases with increasing temperature. The decrease in the exponent g was observed previously for various systems [Garside and Mullin, 1968; Nyvlt and Vaclavu, 1972]. Fig. 8 shows the variation of linear growth rate with $\Delta C/C_s$ with 1.39 mm crystal size. It is shown that growth rates increase with increasing crystal size, but the exponent g decreases. The best estimates of the kinetic parameters in Eqs. 15, 16 and 17 were determined from the experimental data by applying the least-squares multiple regression method, and the parameters obtained are shown in Table 2. A typical presentation of the growth rate correlation represented by Eq. (15) is shown in Fig. 9.

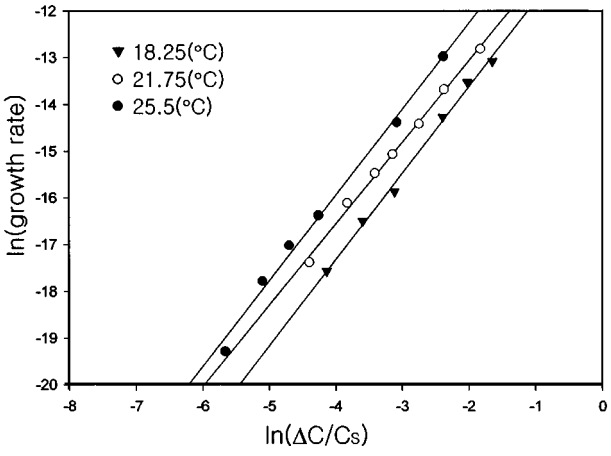

Fig. 7. Linear growth rate vs. relative supersaturation at various saturation temperatures (seed size 1.21 mm).

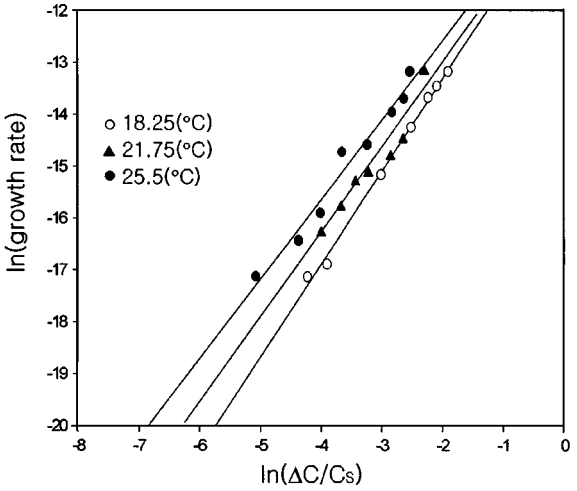

Fig. 8. Linear growth rate vs. relative supersaturation at various saturation temperatures (seed size 1.39 mm).

Table 2. Values of the parameters in Eqs. (15), (16) and (17)

k_d^o	2.298×10^1
b1	−0.281
E_{gd}	1.840×10^4
r	1.984
k_r^0	5.327×10^4
b2	0.134
E_{gr}	2.816×10^4

*Multiple correlation coefficient: 0.961.

To determine the effect of surface reaction step on the crystal growth, Garside [1971] proposed the concept of the surface reaction effectiveness factor defined as

$$\eta_r = \frac{M_g}{k_r\{(C - C_s)/C_s\}^r} \tag{18}$$

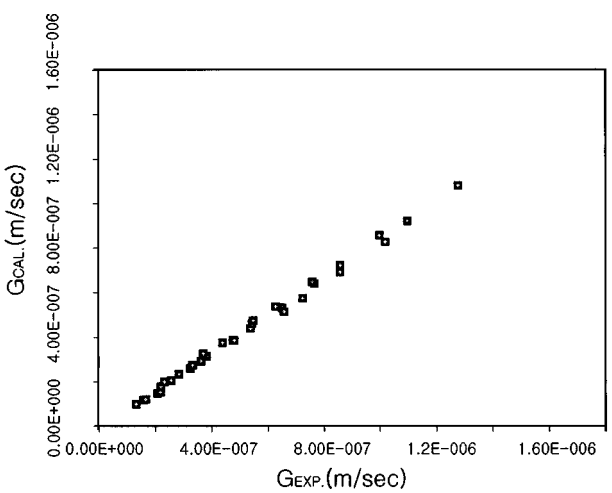

Fig. 9. Growth rate correlation (Eq. (15)).

The effectiveness factor, η_r, tends to unity as the surface reaction step increasingly dominates the growth process. The growth process of AMT becomes more diffusion controlled as the temperature, seed crystal size and supersaturation increase.

4. Programmed Cooling Crystallization

The behavior of a batch cooling crystallizer may be predicted from a theory of programmed cooling crystallization [Jones and Mullin, 1974; Choi and Kim, 1991] based on the moment transformation of the population balance coupled with the material balance. In this work, the controlled cooling crystallization at a constant nucleation rate is considered. The transient temperature may be obtained from a set of equations as follows:

$$\frac{d\mu_0}{dt} = k_n\left(\frac{\Delta C}{C_s}\right)^n = J_n = \text{const.} \tag{19}$$

$$\frac{d\mu_j}{dt} = j\mu_{j-1}\phi\Phi + J_n L_{no}^j \tag{20}$$

$$\frac{dL_s}{dt} = L_s^{b1}\Phi \tag{21}$$

$$\frac{d\theta}{dt} = -\left(\frac{3W_{so}}{L_{so}^3}L_s^{2+b1}\Phi + \frac{d\mu^3}{dt}f_v\rho_c + \frac{d\Delta C}{dt}\right)\left(\frac{dC_s}{d\theta}\right)^{-1} \tag{22}$$

The crystal growth rate, G, may be represented by the empirical expressions.

$$G = aL^{b1}\exp(-E_{gd}/R_gT)\left(\frac{C-C_i}{C_s}\right) = \phi(L)\Phi(c,\theta) \tag{23}$$

where

$$\phi(L) = L^{b1}$$

$$\Phi(c,\theta) = a\exp(-E_{gd}/R_gT)\left(\frac{C-C_i}{C_s}\right)$$

The cooling curves, transient supersaturation and product CSD were computed by using the following values:

L_{so}=0.6 mm, L_{no}=0.06 mm, W_{so}=250 g

$\theta(0)$=25 °C, $\Delta C(0)$=0.02 (Kg/Kg H_2O)

batch time=240 min

The operating policies considered are:

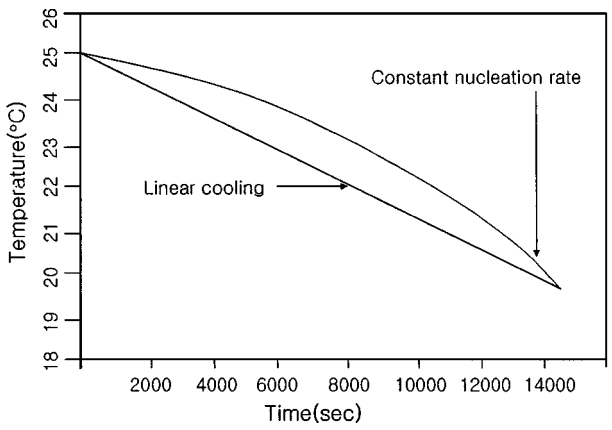

Fig. 10. Theoretical cooling curves for batch crystallization.

Table 3. Theoretical effect of operating policies on the terminal size, mean size and C.V. (Seed Size : 0.6 mm)

Operating policy	Teminal size of seed crystal (mm)	Weight mean size (mm)	C. V. (%)
Constant nucleation	1.000	0.937	21.17
Linear cooling	0.997	0.872	47.82
Natural cooling		<0.8	>50

(1) constant nucleation
(2) linear cooling
(3) natural cooling.

A comparison of the operating policies for batch crystallization is shown in Fig. 10. The statistics of the crystal size distribution calculated from the experimental terminal crystal frequency histogram are presented in Table 3. From the results in Table 3, it could be found that the controlled cooling policies show a significant improvement in the weight mean size.

CONCLUSIONS

1. Kinetics of primary and secondary nucleation of AMT in the AMT-water system were investigated. The Arrhenius equation was used to present the effect of temperature on kinetics of primary and secondary nucleation. The surface energy was inferred from primary nucleation kinetics and its value was 4.16 erg/cm^2.

2. The habit change of AMT crystals during the growth was observed and the values of shape factors were quantified as a function of crystal size.

3. The rate constants of kinetic equations for the diffusion step of crystal growth, and for the surface reaction step of crystal growth were related with temperature and crystal size. The contribution of the diffusion step increased with the increase of temperature, crystal size and supersaturation.

4. The results from this study will do much for finding an optimal operating condition for a batch cooling crystallizer, producing highly pure AMT crystals.

NOMENCLATURE

b : cooling rate [°C/hr]
b_1, b_2 : crystal growth rate size dependence exponent
C : concentration [kg/kg H_2O]
ΔC : concentration difference [kg/kg H_2O]
C_i : interface concentration [kg/kg H_2O]
C_s : saturation concentration [kg/kg H_2O]
D : constant in Eq. (20)
E_{gd} : activation energy for diffusion step [J/mol]
E_{gr} : activation energy for surface reaction step [J/mol]
E_n : activation energy for nucleation [J/mol]
f_s : surface shape factor
f_v : volume shape factor
G : linear growth rate [m/s]

g : growth rate order
J_m : mass nucleation rate [kg/hr kg H_2O]
K : pre-exponential factor in Eq. (10)
k_B : Boltzmann constant
k_d : mass transfer coefficient
k_G : overall linear growth rate constant
k_n : mass nucleation rate constant
k_r : surface reaction rate constant
L : crystal size [m]
M_g : mass growth rate [kg/m^{2}s]
M_W : molecular weight
N : Avogadro's number
n : nucleation order
R_g : gas constant
r : surface reaction order
S : C/Cs
T : absolute temperature [K]
μ_j : jth moment

Greek Letters

β : geometrical factor
γ : surface energy [erg/cm^2]
η_r : effectiveness factor
θ : temperature [^{o}C]
υ : number of ions in a formula unit (=7)
ρ_c : crystal density (=3800 kg/m^3)
τ : induction period

REFERENCES

Choi, C. S. and Kim, I. S., "Growth Kinetics of $(NH_4)_2SO_4$ in the Ternary System $(NH_4)_2SO_4$-NH_4NO_3-H_2O," *Ind. Eng. Chem. Res.*, **29**(7), 1558 (1990).

Choi, C. S. and Kim, I. S., "Controlled Cooling Crystallization of $(NH_4)_2SO_4$ in the Ternary System $(NH_4)_2SO_4$-NH_4NO_3-H_2O," *Ind. Eng. Chem. Res.*, **30**(7), 1588 (1991).

French, G. J. and Sale, F. R., "A Re-investigation of the Thermal Decomposition of Ammonium Paratungstate," *J. Mater. Sci.*, **16**, 3427 (1981).

Garside, J., "The Concept of Effectiveness Factors in Crystal Growth," *Chem. Eng. Sci.*, **26**, 1425 (1971).

Garside, J. and Mullin, J. W., "The Crystallization of Aluminium Potassium Sulphate: A Study in the Assessment of Crystallizer Design Data," *Trans. Instn Chem. Engrs*, **46**, T11 (1968).

Garside, J., Janssen, R. and Bennema, P., "Verification of Crystal Growth Rate Equations," *J. Crystal Growth*, **29**, 353 (1975).

Jones, A. G. and Mullin, J. W., "Crystallization Kinetics of Potassium Sulphate in a Draft-Tube Agitated Vessel," *Trans. Instn Chem. Engrs*, **51**, 302 (1973).

Jones, A. G. and Mullin, J. W., "Programmed Cooling Crystallization of Potassium Sulfate Solutions," *Chem. Eng. Sci.*, **29**, 105 (1974).

Krpata, M. and Söhnel, O., "Formal Crystallization Kinetics," *Collection Czechoslov. Chem. Commun.*, **39**, 2520 (1974).

Mullin, J. W. and Gaska, C., "The Growth and Dissolution of Potassium Sulphate Crystals in a Fluidized Bed Crystallizer," *The Canadian Journal of Chemical Engineering*, **47**, 483 (1969).

Mulline, J. W. and Ang, H. M., "Nucleation Characteristics of Aqueous Nickel Ammonium Sulfate Solutions," *Faraday Discussion Chemical Society*, **61**, 141 (1976).

Nielsen, A. E., "Kinetics of Precipitation," Pergamon, Oxford (1964).

Nyvlt, J., "Evaluation of Experimental Data on Width of Metastable Region in Aqueous Solutions," *Collection Czechoslov. Chem. Commun.*, **37**, 3155 (1972).

Nyvlt, J., "Solid-Liquid Phase Equilibria," Elsevier, Amsterdam (1977).

Nyvlt, J. and Vaclavu, V., "Rate of Growth of Citric Acid Crystals," *Collection Czechoslov. Chem. Commun.*, **37**, 3664 (1972).

Nyvlt, J. and Söhnel, O., "Evaluation of Experimental Data on Width of Metastable Region in Aqueous Solutions," *Collection Czechoslov. Chem. Commun.*, **40**, 511 (1975).